

Evidence for Obscured broad [O III] Components in Type-2 AGN

Xue-Guang Zhang^{*}

School of Physics and technology, Nanjing Normal University, No. 1, Wenyuan Road, Nanjing, 210023, P. R. China

ABSTRACT

In the manuscript, we report evidence on broad [O III] components apparently obscured in Type-2 AGN under the framework of the Unified model, after checking properties of broad [O III] emissions in large samples of Type-1 and Type-2 AGN in SDSS DR12. We can well confirm the statistically lower flux ratios of the broad to the core [O III] components in Type-2 AGN than in Type-1 AGN, which can be naturally explained by stronger obscured broad [O III] components by central dust torus in Type-2 AGN, unless the Unified model for AGN was not appropriate to the narrow emission lines. The results provide further evidence to support broad [O III] components coming from emission regions nearer to central BHs, and also indicate the core [O III] component as the better indicator for central activities in Type-2 AGN, due to few effects of obscuration on the core [O III] component. Considering the broad [O III] components as signs of central outflows, the results provide evidence for strong central outflows being preferentially obscured in Type-2 AGN. Furthermore, the obscured broad [O III] component can be applied to explain the different flux ratios of [O III] λ 5007Å/H β between Type-1 and Type-2 AGN in the BPT diagram.

Key words: galaxies:active - galaxies:nuclei - quasars:emission lines - galaxies:Seyfert

1 INTRODUCTION

Type-1 AGN (broad line Active Galactic Nuclei) and Type-2 AGN (narrow line AGN) having different observational phenomena can be well explained by orientation effects of central dust torus, in the framework of the well-known constantly being revised Unified Model (Antonucci 1993; Netzer 2015; Audibert et al. 2017). Central broad line regions (BLRs) with tens to hundreds of light-days (Kaspi et al. 2000; Bentz et al. 2013; Fausnaugh et al. 2017) to central black holes (BHs) are totally obscured by central dust torus in Type-2 AGN. However, narrow emission line regions (NLRs) with hundreds to thousands of pcs (parsecs) to central BHs (Fischer et al. 2013; Hainline et al. 2014; Sun et al. 2017) lead to expected similar properties of narrow emission lines in both Type-1 and Type-2 AGN. Therefore, properties of narrow emission lines can be well applied to estimate central activities in Type-2 AGN, such as the reported strong linear correlation between AGN power-law continuum luminosity and [O III] luminosity (Zakamska et al. 2003; Heckman & Best 2014).

Recently, Zhang et al. (2017) have reported the broad [O III] emission regions nearer to central BLRs, based on the tighter correlation between AGN continuum luminosity and luminosity of broad [O III] components, through a larger sample of SDSS (Sloan Digital Sky Survey) blue quasars (Type-1 AGN). Actually, broad [O III] components in AGN have been studied for more than three decades. Greene & Ho (2005) have shown further effects of central BH potential on broad [O III] components. Similar blue broad [O III] components can also be found in Komossa et al. (2008); Shen et al. (2011); Bennert et al. (2018); Schmidt et al. (2018). More recently, DiPompeo et al. (2018) have shown interesting results on broader and more blue-shifted broad [O III] emissions in the obscured AGN indicating more powerful AGN-driven outflows, a probable challenge to the Unified Model of AGN. Furthermore, besides kinematic study on broad [O III] com-

ponents, geometric properties of broad [O III] components have been also well studied in the literature. Sun et al. (2017) have shown that the extended narrow emission regions related to broad [O III] components have typically smaller sizes than the sizes of normal [O III] emission regions expected by AGN luminosity and/or [O III] luminosity (Liu et al. 2013; Hainline et al. 2013, 2014). Besides plenty of research results on properties of broad [O III] emissions in AGN in the literature, we here will focus on one another interesting point on broad [O III] emissions in AGN.

If broad [O III] components were nearer to central BHs, broad [O III] components could be more likely to be obscured by central dust torus in Type-2 AGN under the framework of the Unified model. The results could provide further information on linkage between narrow and broad emission lines, and furthermore, could provide further clues on AGN selection criterion through applications of narrow emission line ratios in BPT diagrams (Baldwin et al. 1981; Kauffmann et al. 2003; Kewley et al. 2006, 2013, 2019; Zhang et al. 2020) with line ratios on [O III] lines. Meanwhile, further considerations should be given on applications of [O III] properties to trace central AGN activities in Type-2 AGN. The manuscript is organized as follows. In Section 2, we show our main data samples of both Type-1 and Type-2 AGN. In Section 3, we show our main results and necessary discussions. In Section 4, we give our final conclusions. And in the manuscript, we have adopted the cosmological parameters of $H_0 = 70 \text{ km} \cdot \text{s}^{-1} \text{ Mpc}^{-1}$, $\Omega_\Lambda = 0.7$ and $\Omega_m = 0.3$.

2 MAIN SAMPLES OF TYPE-2 AGN AND TYPE-1 AGN

In the manuscript, Type-1 AGN are collected from the SDSS pipeline classified quasars. Type-2 AGN are collected from the SDSS sub-classified AGN in SDSS pipeline classified main galaxies based on the MPA-JHU measurements

arXiv:2101.07904v1 [astro-ph.GA] 20 Jan 2021

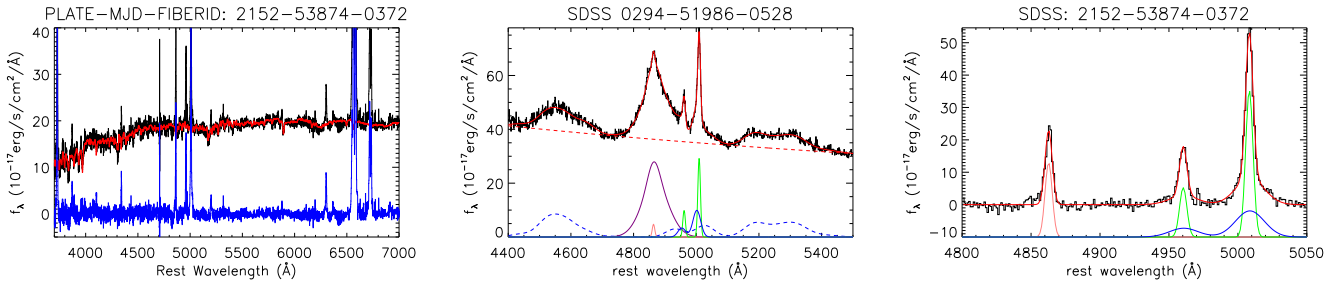


Figure 1. Left panel shows an example on the SSP method determined stellar components in the Type-2 AGN SDSS 2152-53874-0372. Solid lines in black, red and blue show the observed spectrum, the best determined stellar components and the pure line spectrum, respectively. Middle and right panels show two examples on the best fitted results to the emission lines around $H\beta$ in the Type-1 AGN SDSS 0294-51986-0528 and in the Type-2 AGN SDSS 2152-53874-0372. In middle and right panels, solid lines in black and red show the line spectrum and the best fitted results, solid pink line shows the determined narrow $H\beta$, solid lines in green and blue show the determined core and broad $[O\ III]$ components, respectively. In middle panel, dashed red line shows the determined power law continuum emissions, solid purple line shows the determined broad $H\beta$ component, dashed blue line shows the determined optical $Fe\ II$ emissions, respectively.

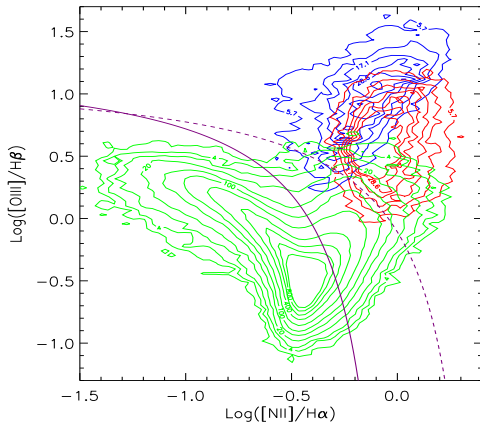


Figure 2. BPT diagram for the 5437 Type-1 AGN (contour in blue) and for the 6587 Type-2 AGN (contour in red) with reliable narrow emission lines. Solid and dot-dashed purple lines represent the dividing lines discussed in Kauffmann et al. (2003); Kewley et al. (2006). Contour in green shows the results based on more than 240000 narrow-emission-line galaxies in SDSS DR12.

(http://www.sdss3.org/dr9/algorithms/galaxy_mpa_jhu.php).

Accepted the criterion of redshift less than 0.3, there are 12342 Type-1 AGN from SDSS quasars and 16269 Type-2 AGN from SDSS main galaxies collected from SDSS DR12. Then, emission line parameters are measured as follows.

For Type-2 AGN and a small number of Type-1 AGN, of which spectra have clear host galaxy contaminations, the widely accepted SSP (Simple Stellar Population) method has been firstly applied to subtract the stellar lights, in order to find more accurate emission line properties. Detailed descriptions of the SSP method can be found in Bruzual & Charlot (2003); Kauffmann et al. (2003); Cid Fernandes et al. (2005) etc.. The same procedure has been applied in our previous studies in Zhang (2014); Zhang et al. (2016); Rakshit et al. (2017); Zhang et al. (2019), etc.. We do not discuss the SSP method any more, but the left panel of Fig. 1 shows an example on the SSP method determined stellar components in the Type-2 AGN with PLATE-MJD-FIBERID = 2152-53874-0372.

After subtractions of the stellar lights, line parameters can be well measured. The emission lines are mainly considered around $H\beta$ (rest wavelength from 4400Å to 5600Å) and around $H\alpha$ (rest

wavelength from 6250Å to 6850Å), which are fitted simultaneously by the following model functions through the Levenberg-Marquardt least-squares minimization technique (the MPFIT package), similar as what we have done in Zhang et al. (2016, 2017). There are two (or more if necessary, after checking the fitted results) broad Gaussian functions applied to describe each broad Balmer line (especially in Type-1 AGN), one narrow Gaussian function applied to each narrow emission line including narrow Balmer lines, $[O\ III]$, $[N\ II]$, $[O\ I]$ and $[S\ II]$ doublets, and two additional Gaussian components applied to describe probably broad components of $[O\ III]$ doublet (broad $[O\ III]$ components), one broad Gaussian function applied to describe weak $He\ II$ line, two power law functions applied to describe probable AGN continuum emissions underneath the broad $H\beta$ and underneath the broad $H\alpha$, and the $Fe\ II$ template discussed in Kovacevic et al. (2010) applied to describe optical $Fe\ II$ lines (especially for Type-1 AGN). When the model functions are applied, the following restrictions have been accepted, (1) narrow emission lines have the same redshift, (2) corresponding broad components in broad Balmer lines have the same redshift, (3) flux ratio of the $[O\ III]$ ($[N\ II]$) doublet is fixed to the theoretical value 3, (4) there are the same line widths of narrow Balmer lines ($[O\ III]$ or $[O\ I]$ or $[N\ II]$ or $[S\ II]$ doublets), but different line widths for different narrow lines. Middle and right panels of Fig. 1 show two examples on the best fitted results to the emission lines around $H\beta$.

Based on the measured parameters, two criteria have been accepted to collect Type-2 AGN with reliable narrow emission lines but no broad Balmer lines. First, measured stellar velocity dispersions and line parameters of the narrow emission lines ($[O\ III]\lambda 5007\text{Å}$ (at least core $[O\ III]$ components), narrow Balmer lines and $[N\ II]\lambda 6583\text{Å}$) are at least 5 times larger than their corresponding uncertainties. Second, measured line fluxes of broad Balmer lines are less than 5 times of the corresponding uncertainties. Then, there are 6587 Type-2 AGN collected. Moreover, two criteria have been accepted to collect Type-1 AGN with reliable narrow and broad emission lines. First, the measured continuum luminosity and line parameters of broad Balmer components are at least 5 times larger than their corresponding uncertainties. Second, the measured line parameters of $[O\ III]\lambda 5007\text{Å}$ (at least core $[O\ III]$ components), narrow Balmer lines and $[N\ II]\lambda 6583\text{Å}$ are at least 5 times larger than their corresponding uncertainties. Then, there are 5437 Type-1 AGN collected. Fig. 2 shows the BPT diagram of flux ratio of $[O\ III]\lambda 5007\text{Å}$ to narrow $H\beta$ ($O3HB$) versus flux ratio of $[N\ II]\lambda 6583\text{Å}$ to narrow $H\alpha$ ($N2HA$) for the collected 5437 Type-1 AGN and 6587 Type-2 AGN. Here, the

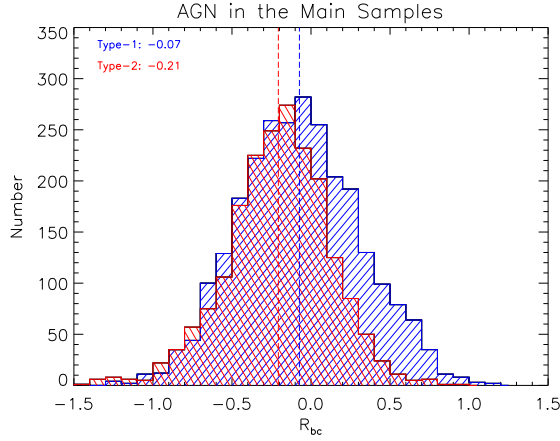


Figure 3. Distributions of R_{bc} of the Type-1 AGN (in blue) and the Type-2 AGN (in red) in the main samples. Vertical dashed lines in blue and in red show the mean value positions of the Type-1 and Type-2 AGN, respectively. Mean value of each distribution is marked in the top-left corner.

[O III] λ 5007Å flux means the total [O III] line flux. The collected objects can be safely classified as AGN, based on the dividing lines well discussed in Kauffmann et al. (2003); Kewley et al. (2006, 2013).

Finally, among the 5437 Type-1 AGN and the 6587 Type-2 AGN, the following criteria are applied to create our main samples of Type-1 and Type-2 AGN with reliable broad [O III] components: the measured line flux and line width (second moment) of both the core and the broad [O III] components are at least 5 times larger than their corresponding uncertainties. Here, the determined [O III] component with larger second moment is the broad [O III] component. Then, in final main samples, there are 2621 Type-1 AGN and 1987 Type-2 AGN, with reliable broad [O III] components.

3 MAIN RESULTS AND DISCUSSIONS

Based on the determined core and broad [O III] components, properties of the parameter $R_{bc} = \log(L_b) - \log(L_c)$ have been checked and shown in Fig. 3, where L_b and L_c represent luminosities of the broad and the core [O III] components, respectively. The mean R_{bc} are about -0.07 and -0.21 in the Type-1 and Type-2 AGN, respectively. And the Student’s T-statistic technique shows that the different mean values are significant with levels higher than 10σ . Therefore, there could be intrinsic different properties of [O III] components between Type-1 and Type-2 AGN.

In order to show more accurate results with contaminations as less as possible, The following effects have been mainly considered. As the results shown in the top panels of Fig. 4, the Type-1 and Type-2 AGN have much different distributions of redshift, O3HB and N2HA. The different redshift distribution will lead to much different luminosity properties of [O III] components. And, the different distributions of O3HB and N2HA will indicate much different central activities between the Type-1 and Type-2 AGN in the main samples. In order to totally ignore effects of different distributions of redshift and emission line ratios between the Type-1 and Type-2 AGN, a simple method has been considered, by comparing Type-1 and Type-2 AGN in two subsamples which have the same distributions of redshift and emission line ratios (called BPT/redshift-matched samples).

Based on the distributions of redshift, O3HB_c (flux ratio of the core [O III] component to narrow H β) and N2HA of the 2621 Type-1 AGN and the 1987 Type-2 AGN in the main samples, 667 Type-1

AGN and 667 Type-2 AGN are randomly collected from the main samples to create the two BPT/redshift-matched samples which have the same distributions of redshift, O3HB_c and N2HA, as the results shown in the bottom panels of Fig. 4. Here, not O3HB but O3HB_c is applied, because of the broad [O III] components in Type-2 AGN probably obscured. Based on the strong correlation between core [O III] luminosity and AGN continuum luminosity in (Zhang et al. 2017), central activities can also be well traced by applications of core [O III] components. The two-sided Kolmogorov-Smirnov statistic technique has been applied to confirm the same distributions of redshift, O3HB_c and N2HA with significance levels higher than 92% between the 667 Type-1 AGN and the 667 Type-2 AGN in the BPT/redshift-matched samples.

Then, the parameter R_{bc} has been re-checked in the top panel of Fig. 5 for the AGN in the BPT/redshift-matched samples, with the mean R_{bc} of about -0.02 and -0.26 in the 667 Type-1 AGN and in the 667 Type-2 AGN, respectively. The difference is more apparent than the results for the AGN in the main samples shown in Fig. 3. And the different mean values have Student’s T-statistic determined significance levels higher than 10σ . Furthermore, the bottom panel of Fig. 5 shows the luminosity distribution of L_c for the AGN in the BPT/redshift-matched samples with the same mean values. And through the two-sided Kolmogorov-Smirnov statistic technique, the Type-1 and Type-2 AGN in the BPT/redshift-matched samples have the same L_c distributions with significance levels higher than 60%. Therefore, intrinsic different broad [O III] components lead to the different R_{bc} between the Type-1 and Type-2 AGN, and the direct and natural explanation to the lower L_b in Type-2 AGN is that the broad [O III] emissions have been obscured, under the framework of the Unified model for AGN.

Before proceeding further, there is one point we should note. In the manuscript, we do not discuss the effects of beam smearing on our results. The beam smearing effects have been discussed for more than five decades (Begeman 1989; Wright et al. 2009; Green et al. 2010; Stott et al. 2016; Zheng et al. 2017), especially on kinematic properties through integral-filed spectra. The more recent discussions on the effects of beam smearing can be found in Husemann et al. (2016, 2020). For the SDSS optical fiber spectra discussed in the manuscript, it is hard to clearly determine and remove the beam smearing effects on emission lines, due to loss of physical information of spatially resolved velocity field. In order to roughly check the beam smearing effects, line width (second moment) difference $\Delta_{bc} = \sigma_b - \sigma_c$ between the broad and core [O III] components can be roughly applied to show properties of central velocity gradient. Then, the dependence of Δ_{bc} on the parameter R_{bc} have been checked in the Type-1 and Type-2 AGN in the BPT/redshift-matched samples. The Spearman rank correlation coefficients are about -0.12 and 0.04 for the Type-1 and Type-2 AGN, respectively, strongly indicating no dependence of the parameter of R_{bc} on central velocity gradient in Type-1 AGN nor in Type-2 AGN. Therefore, the beam smearing effects have few effects on our final results, even there are different beam smearing effects between Type-1 and Type-2 AGN due to different orientation effects.

Meanwhile, we provide further discussions on the obscured broad [O III] components in Type-2 AGN. First, similar as results discussed in Zhang et al. (2017), the core rather than the broad [O III] components (or the total [O III]) could be the better indicator to central activities in Type-2 AGN. Through the parameter of R_{bc} different in Type-1 and Type-2 AGN, we can roughly estimate that about 50% of broad [O III] emissions are obscured in Type-2 AGN. Therefore, the classification by narrow emission line ratios in the BPT diagram should lead to lower O3HB, if total [O III] lines were considered.

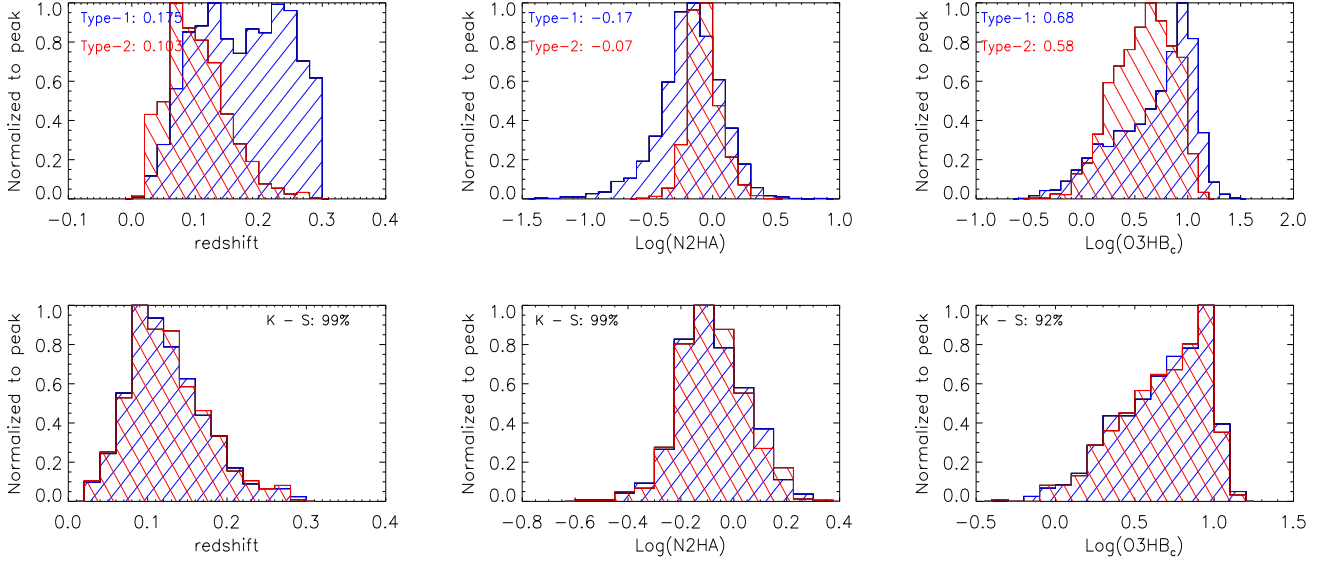


Figure 4. Distributions of redshift, N2HA and O3HB_c of the Type-1 AGN (in blue) and the Type-2 AGN (in red) in the main samples (top panels) and in the BPT/redshift-matched samples (bottom panels). In each top panel, mean values of the distributions are marked in the top-left corner. In each bottom panel, the calculated Kolmogorov-Smirnov statistical significance level is marked in the top-left corner.

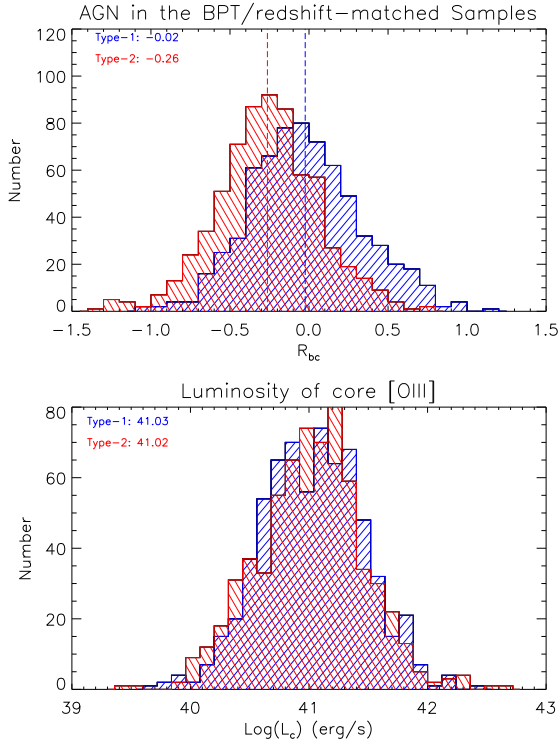


Figure 5. Top panel shows the results similar as those in Fig. 3, but for the AGN in the BPT/redshift-matched samples. Bottom panel shows luminosity distributions of $\text{log}(L_c)$ of the AGN in the BPT/redshift-matched samples.

Second, based on similar intrinsic properties of [O III] emission components expected by the framework of the Unified model for AGN, there are few selection effects on the results shown in Fig. 5. Third, based on the results shown in Fig. 2, the Type-2 and Type-1

AGN have statistical different O3HB in the BPT diagram, with mean $\text{log}(O3HB)$ about 0.91 and 0.71 in the Type-1 and Type-2 AGN, respectively. Once, we simply accepted that about 50% of broad [O III] emissions are obscured in Type-2 AGN by properties of R_{bc} , we could expect the intrinsic flux ratio of $\text{log}(O3HB)$ in Type-2 AGN about $0.71 + \text{log}(1.5) \sim 0.89$ similar as the mean value of 0.91 of the Type-1 AGN.

As the direct and natural explanation on weaker broad [O III] emissions in Type-2 AGN by obscuration, it will be interesting to consider sources of the obscurations. Central dust torus in AGN could be preferred, rather than randomly moving dust clouds in central regions, otherwise, there should be similar obscurations on broad [O III] emissions in Type-1 AGN. As discussed properties of central dust torus in [Burtscher et al. \(2015\)](#); [Gandhi et al. \(2015\)](#); [Zhuang et al. \(2017\)](#), opening angle could be around $\theta \sim 40 - 60^\circ$ in AGN, and the dust sublimation radius $R_{sub} \propto 1.3\text{pc} \times L^{0.5}$ could be accepted as the radius of dust torus. In order to provide appropriate obscurations on broad [O III] emissions in Type-2 AGN, scales of the distance R_{B3} of broad [O III] emission regions to central BHs could be simply around $R_{B3} \sim R_{sub} \times \tan(\theta/2)$. If a global mean value of $\theta \sim 25^\circ$ was accepted, we will have $R_{B3} \sim 0.6\text{pc}(L_{UV}/10^{46}\text{erg/s})^{0.5}$. Meanwhile, the BLRs size can be well estimated as $R_{BLRs} \propto 34(L_{opt}/10^{44}\text{erg/s})^{0.5}\text{light-days}$ ([Kaspi et al. 2000](#); [Bentz et al. 2013](#)). Then, an oversimplified result can be expected $R_{B3} \sim 20 \times R_{BLRs}$, about 3 magnitudes smaller than the distance of common [O III] emission regions to central BHs ([Hainline et al. 2013](#)), providing interesting clues on very broader [O III] components in AGN. Certainly, we should note that the expression $R_{B3} \sim 20 \times R_{BLRs}$ is estimated through tremendously oversimplified structures of central dust torus, however, the results can provide structure information on the potential obscured broad [O III] emission regions much nearer to central BHs between BLRs and normal NLRs in AGN, as expected by properties of kinematically-disturbed broad [O III] regions related to outflows discussed in [Sun et al. \(2017\)](#).

Before the end of the section, line intensity properties rather than kinematic properties of broad and core [O III] components are mainly considered in the manuscript. More detailed discussions can be found on kinematic properties of gas outflows through properties of [O III] emissions in Type-2 AGN in Woo et al. (2016, 2017) and in Type-1 AGN in DiPompeo et al. (2018). Here, we simply check the correlation between stellar velocity dispersions (σ_*) and line widths of broad (σ_b) and core [O III] (σ_c) components in the Type-2 AGN, and find that the mean ratios of σ_* to σ_c and of σ_* to σ_b are about 1.05 and 0.27, respectively. The results well consistent with the reported results in Woo et al. (2016) strongly indicate broad [O III] components tightly related to outflowing gases in Type-2 AGN. And the wider broad [O III] components can be well expected due to the broad [O III] emission regions with deeper gravitational potential nearer to central BHs. Moreover, we check the expected positive correlation between line width of the broad [O III] components and the [O III] luminosity in Type-1 and Type-2 AGN, such as the positive correlations shown in Figure 6 in DiPompeo et al. (2018). Here, the broad [O III] luminosity is applied to trace the central AGN luminosity as discussed in Zhang et al. (2017) in Type-1 AGN, but the core [O III] luminosity is applied in Type-2 AGN. Then, positive correlations can be found with Spearman rank correlation coefficients about 0.40 with $P_{\text{null}} \sim 10^{-23}$ and about 0.32 with $P_{\text{null}} \sim 10^{-17}$ in the Type-1 AGN and in the Type-2 AGN, respectively. It is clear that the kinematic properties of the collected Type-1 and Type-2 AGN are consistent with the reported results in the literature.

4 CONCLUSIONS

Finally, we give our main conclusions as follows. Based on the SDSS high quality spectra of large samples of Type-1 and Type-2 AGN with reliable broad [O III] components, different properties of broad [O III] components can be confirmed between the Type-1 and Type-2 AGN: statistically lower broad [O III] luminosities and statistically lower R_{bc} (flux ratio of the broad to the core [O III] component) in the Type-2 AGN, after considering necessary effects. The results indicate stronger obscuration on the broad [O III] components in the Type-2 AGN due to broad [O III] emission regions nearer to central BHs, under the framework of the Unified model for AGN. Considering the broad [O III] components as robust signs of central outflows, the results provide evidence for obscured central outflows in Type-2 AGN. Moreover, rather than total [O III] lines, the core [O III] components can be treated as the better indicator of central activities in Type-2 AGN, due to few effects of obscuration on the core [O III] components. Furthermore, the obscured broad [O III] components can be well applied to explain the different flux ratios of O3HB in the BPT diagram between Type-1 and Type-2 AGN.

ACKNOWLEDGEMENTS

Zhang gratefully acknowledges the anonymous referee for giving us constructive comments and suggestions greatly improving our paper. Zhang gratefully thanks the kind financial support from Nanjing Normal University and the kind grant support from NSFC-11973029. This paper has made use of the data from the SDSS projects. The SDSS-III web site is <http://www.sdss3.org/>. SDSS-III is managed by the Astrophysical Research Consortium for the Participating Institutions of the SDSS-III Collaboration.

DATA AVAILABILITY

The data underlying this article will be shared on reasonable request to the corresponding author (xgzhang@nynu.edu.cn).

REFERENCES

- Antonucci, R., 1993, *ARA&A*, 31, 473
 Audibert, A.; Riffel, R.; Sales, D. A.; Pastoriza, M. G.; Ruschel-Dutra, D., 2017, *MNRAS*, 464, 2139
 Baldwin, J. A.; Phillips, M.; Terlevich, R., 1981, *PASP*, 93, 5
 Begeman, K. G., 1989, *A&A*, 223, 47
 Bennert, V. N.; Loveland, D.; Donohue, E.; et al., 2018, *MNRAS*, 481, 138
 Bentz, M. C., et al., 2013, *ApJ*, 767, 149
 Burtcher, L.; Orban de Xivry, G.; Davies, R. I.; et al., 2015, *A&A*, 578, 47
 Bruzual, G.; Charlot, S. 2003, *MNRAS*, 344, 1000
 Cid Fernandes, R.; Mateus, A.; Sodre, L.; Stasinska, G.; Gomes, J. M., 2005, *MNRAS*, 358, 363
 DiPompeo, M. A.; Hickox, R. C.; Carroll, C. M.; et al., 2018, *ApJ*, 856, 76
 Fausnaugh, M. M., et al., 2017, *ApJ*, 840, 97
 Fischer, T. C.; Crenshaw, D. M.; Kraemer, S. B., Schmitt, H. R., 2013, *ApJS*, 209, 1
 Gandhi, P.; Honig, S. F.; Kishimoto, M., 2015, *ApJ*, 812, 113
 Green, A. W.; Glazebrook, K.; McGregor, P. J.; et al., 2010, *Natur*, 467, 684
 Greene, J. E.; Ho, L. C., 2005, *ApJ*, 627, 721
 Hainline, K. N.; Hickox, R.; Greene, J. E.; Myers, Adam D.; Zakamska, N. L., 2013, *ApJ*, 774, 145
 Hainline, K. N., et al., 2014, *ApJ*, 787, 65
 Heckman, T. M.; Best, P. N., 2014, *ARA&A*, 52, 589
 Husemann, B.; Scharwacher, J.; Bennert, V. N.; Mainieri, V.; Woo, J.; D. Kakkad, D., 2016, *A&A*, 594, 44
 Husemann, B.; Heidt, J.; De Rosa, A.; et al., 2020, *A&A*, 639, 117
 Kaspi, S., et al., 2000, *ApJ*, 533, 631
 Kauffmann, G., et al. 2003, *MNRAS*, 346, 1055
 Kewley, L. J., Groves, B., Kauffmann, G., Heckman, T., 2006, *MNRAS*, 372, 961
 Kewley, L. J., et al., 2013, *ApJ*, 774, 100
 Kewley, L. J.; Nicholls, D. C.; Sutherland, R. S., 2019, *ARA&A*, 57, 511
 Komossa, S.; Xu, D.; Zhou, H.; Storchi-Bergmann, T.; Binette, L., *ApJ*, 2008, 680, 926
 Kovacevic, J.; Popovic, L. C.; Dimitrijevic, M. S., 2010, *ApJS*, 189, 15
 Liu, G.; Zakamska, N. L.; Greene, J. E.; Nesvadba, N. P. H.; Liu, X., 2013, *MNRAS*, 436, 2576
 Netzer, H., 2015, *ARA&A*, 53, 365
 Rakshit, S.; Stalin, C. S.; Chand, H.; Zhang, X. G., 2017, *ApJS*, 229, 39
 Schmidt, E. O.; Oio, G. A.; Ferreiro1, D.; Vega1, L.; Weidmann, W., 2018, *A&A*, 615, 13
 Shen, Y.; Richards, G. T.; Strauss, M. A.; et al., 2011, *ApJS*, 194, 45
 Stott, J. P.; Swinbank, A. M.; L. Johnson, H. L.; et al., 2016, *MNRAS*, 457, 1888
 Sun, A. L.; Greene, J. E.; Zakamska, N. L., 2017, *ApJ*, 835, 222
 Woo, J.; Bae, H.; Son, D.; Karouzos, M., 2016, *ApJ*, 817, 108
 Woo, J.; Son, D.; Bae, H., 2017, *ApJ*, 839, 120
 Wright, S. A.; Larkin, J. E.; Law, D. R.; Steidel, C. C.; Shapley, A. E.; Erb, D. K.; 2009, *ApJ*, 699, 421
 Zakamska, N. L., et al., 2003, *AJ*, 126, 2125
 Zhang, X. G., 2014, *MNRAS*, 438, 557
 Zhang, X. G.; Feng, L. L., 2016, *MNRAS*, 457, 3878
 Zhang, X. G.; Feng, L. L., 2017, *MNRAS*, 468, 620
 Zhang, X. G.; Bao, M.; Yuan, Q. R., 2019, *MNRAS Letter*, 490, 81
 Zhang, X. G.; Feng, Y. Q.; Chen, H.; Yuan, Q. R., 2020 *ApJ in press*
 Zheng Z.; Wang H.; Ge J.; et al., 2017, *MNRAS*, 465, 4572
 Zhuang, M.; Ho, L. C.; Shangguan, J., 2018, *ApJ*, 862, 118

This paper has been typeset from a $\text{\TeX}/\text{\LaTeX}$ file prepared by the author.